Inorganic Chemistry
Article

Inorg. Chem. **2009**, *48*, 6641–6651 **6641**
DOI: 10.1021/ic900616c

Magnesium Substitutions in Rare-Earth Metal Germanides with the Orthorhombic Gd_5Si_4-type Structure. Synthesis, Crystal Chemistry, and Magnetic Properties of $RE_{5-x}Mg_xGe_4$ (*RE* = Gd−Tm, Lu, and Y)

Paul H. Tobash and Svilen Bobev*

Department of Chemistry and Biochemistry, University of Delaware, Newark, Delaware 19716

Joe D. Thompson and John L. Sarrao

Los Alamos National Laboratory, Los Alamos, New Mexico 87545

Received March 30, 2009

A series of magnesium-substituted rare-earth metal germanides with a general formula $RE_{5-x}Mg_xGe_4$ ($x \approx 1.0-2.3$; *RE* = Gd−Tm, Lu, Y) have been synthesized by high-temperature reactions and structurally characterized by single-crystal X-ray diffraction. These compounds crystallize with the common Gd_5Si_4 type structure in the orthorhombic space group *Pnma* (No. 62; $Z = 4$; Pearson's code *oP*36) and do not appear to undergo temperature-induced crystallographic phase transitions down to 120 K. Replacing rare-earth metal atoms with Mg, up to nearly 45% at., reduces the valence electron count and is clearly expressed in the subtle changes of the Ge−Ge and metal−metal bonding. Magnetization measurements as a function of the temperature and the applied field reveal complex magnetic structures at cryogenic temperatures and Curie−Weiss paramagnetic behavior at higher temperatures. The observed local moment magnetism is consistent with RE^{3+} ground states in all cases. In the magnetically ordered phases, the magnetization cannot reach saturation in fields up to 50 kOe. The structural trends across the series and the variations of the magnetic properties as a function of the Mg content are also discussed.

Introduction

The rare-earth metal (*RE*) silicides and germanides crystallizing with the orthorhombic Gd_5Si_4, Pu_5Rh_4, and Sm_5Ge_4 types (*Pnma*, Pearson's code *oP*36), as well as the closely related tetragonal Zr_5Si_4 type ($P4_12_12$, Pearson's code *tP*36), monoclinic $Gd_5Si_2Ge_2$ ($P2_1/c$, Pearson's code *mP*36), and $U_2Mo_3Si_4$ types ($P2_1/c$, Pearson's code *mP*18), have been extensively studied in the last 10 years.[1−13] The interest in these materials was instigated by the discovery in 1997 of a giant magnetocaloric effect in $Gd_5Si_2Ge_2$, associated with the interplay between characteristic crystallographic distortions and a spontaneous magnetic order.[1] Ever since then, there have been numerous studies confirming that the magnetic order in $Gd_5Si_2Ge_2$ is coupled with a reversible, first-order

*To whom correspondence should be addressed. E-mail: bobev@udel.edu. Phone: (302) 831-8720. Fax: (302) 831-6335.

(1) Pecharsky, V. K.; Gschneidner, K. A.Jr. *Phys. Rev. Lett.* **1997**, *78*, 4494.
(2) (a) Choe, W.; Pecharsky, V. K.; Pecharsky, A. O.; Gschneidner, K. A. Jr.; Young, V. G.Jr.; Miller, G. J. *Phys. Rev. Lett.* **2000**, *84*, 4617. (b) Morellon, L.; Algarabel, P. A.; Ibarra, M. R.; Blasco, J.; García-Landa, B. *Phys. Rev. B.* **1998**, *58*, R14721. (c) Pecharsky, V. K.; Pecharsky, A. O.; Gschneidner, K. A. Jr. *J. Alloys Compd.* **2002**, *344*, 362. (d) Mozharivskyj, Y.; Pecharsky, A. O.; Pecharsky, V. K.; Miller, G. J. *J. Am. Chem. Soc.* **2005**, *127*, 317. (e) Levin, E. M.; Gschneidner, K. A.Jr.; Pecharsky, V. K. *Phys. Rev. B* **2002**, *65*, 214427. (f) Magen, C.; Arnold, Z.; Morellon, L.; Skorokhod, Y.; Algarabel, P. A.; Ibarra, M. R.; Kamarad, J. *Phys. Rev. Lett.* **2003**, *91*, 207202-1.
(3) (a) Gschneidner, K. A.Jr.; Pecharsky, V. K.; Tsokol, A. O. *Rep. Prog. Phys.* **2005**, *68*, 1479. (b) Levin, E. M.; Pecharsky, V. K.; Gschneidner, K. A.Jr. *Phys. Rev. B* **1999**, *60*, 7993. (c) Levin, E. M.; Pecharsky, V. K.; Gschneidner, K. A.Jr. *J. Magn. Magn. Matter.* **2000**, *210*, 181. (d) Levin, E. M.; Pecharsky, V. K.; Gschneidner, K. A.Jr. *Phys. Rev. B* **2001**, *63*, 174110.
(4) (a) Morellon, L.; Algarabel, P. A.; Magen, C.; Ibarra, M. R. *J. Magn. Magn. Mater.* **2001**, *237*, 119. (b) Morellon, L.; Blasco, J.; Algarabel, P. A.; Ibara, M. R. *Phys. Rev. B* **2000**, *62*, 1022. (c) Magen, C.; Morellon, L.; Algarabel, P. A.; Marquina, C.; Ibara, M. R. *J. Phys.: Condens. Matter* **2003**, *15*, 2389. (d) Morellon, L.; Stankiewicz, J.; Garcia-Landa, B.; Algarabel, P. A.; Ibara, M. R. *Appl. Phys. Lett.* **1998**, *73*, 3462.
(5) (a) Choe, W.; Pecharsky, A. O.; Wörle, M.; Miller, G. J. *Inorg. Chem.* **2003**, *42*, 8223. (b) Miller, G. J. *Chem. Soc. Rev.* **2006**, *35*, 799. (c) Pecharsky, A. O.; Gschneidner, K. A.Jr.; Pecharsky, V. K.; Schindler, C. E. *J. Alloys Compd.* **2002**, *338*, 126. (d) Pecharsky, V. K.; Samolyuk, G. D.; Antropov, V. P.; Pecharsky, A. O.; Gschneidner, K. A.Jr. *J. Solid State Chem.* **2003**, *171*, 57. (e) Choe, W.; Miller, G. J.; Meyers, J.; Chumbley, S.; Pecharsky, A. O. *Chem. Mater.* **2003**, *15*, 1413.
(6) Pecharsky, A. O.; Gschneidner, K. A.Jr.; Pecharsky, V. K.; Schlagel, D. L.; Lograsso, T. A. *Phys. Rev. B* **2004**, *70*, 144419.
(7) Pereira, A. M.; Sousa, J. B.; Araujo, J. P.; Magen, C.; Algarabel, P. A.; Morellon, L.; Marquina, C.; Ibarra, M. R. *Phys. Rev. B* **2008**, *77*, 134404.
(8) (a) Ahn, K.; Tsokol, A. O.; Mozharivskyj, Yu.; Gschneidner, K. A.Jr.; Pecharsky, V. K. *Phys. Rev. B* **2005**, *72*, 054404. (b) Ritter, C.; Morellon, L.; Algarabel, P. A.; Magen, C.; Ibarra, M. R. *Phys. Rev. B* **2002**, *65*, 094405. (c) Zou, M.; Pecharsky, V. K.; Gschneidner, K. A.Jr.; Schlagel, D. L.; Lograsso, T. A. *Phys. Rev. B* **2008**, *78*, 014435.
(9) Mozharivskyj, Y.; Choe, W.; Pecharsky, A. O.; Miller, G. J. *J. Am. Chem. Soc.* **2003**, *125*, 15183.
(10) Wu, L.-M.; Kim, S.-H.; Seo, D.-K. *J. Am. Chem. Soc.* **2005**, *127*, 15682.
(11) Tobash, P. H.; Bobev, S. *J. Am. Chem. Soc.* **2006**, *128*, 3532.
(12) Misra, S; Miller, G. J. *J. Am. Chem. Soc.* **2008**, *130*, 13900.
(13) Svitlyk, V.; Miller, G. J.; Mozharivskyj, Y. *J. Am. Chem. Soc.* **2009**, *1301*, 2367.

Published on Web 05/06/2009

phase transition, which can be controlled by temperature, pressure, magnetic field, and composition.[2] Subsequently, other interesting phenomena, such as a giant magnetoresistance and a colossal magnetostriction have also been found within the realm of the rare-earth metal−tetrel element systems.[2−8]

What makes the structures in question even more attractive, from both a fundamental and a practical perspective, is the fact that they are amenable to substitutions by many different elements. For example, related compounds can be made by replacements of both the tetrel element and the rare-earth metal, as evidenced by very recent experimental and theoretical work on $RE_5(Si_xGe_{1-x})_4$,[3−8] $Gd_5(Ga_xGe_{1-x})_4$ with $0 \leq x \leq 0.55$,[9] $RE_{5-x}Ca_xGe_4$ with $x \approx 3.0-3.5$ (RE = La, Ce),[10] $Yb_{5-x}Mg_xGe_4$ ($x \approx 1.0-1.2$),[11] $(Gd_{5-x}Y_x)Si_4$,[12] and $Gd_5(Si_{1-x}P_x)_4$ with $0 \leq x \leq 0.5$.[13] These reports emphasize that both the structure and the properties are intimately affected by small changes in the valence electron concentrations, as well as the cation−anion, cation−cation interactions, and/or the packing efficiency. They also provide evidence that the bonding arrangements in the compounds under consideration can be continuously varied from the formally electron-rich to the electron-deficient region.[14] Such phenomenology creates many possibilities for rational modifications of the crystal structures and tuning of the magnetic and electronic properties through systematic cation/anion substitutions, ideas that have already been exploited in the cases of $Gd_5(Si_xSn_{1-x})_4$,[15] $Gd_5Si_{3.5-x}Ge_xSn_{0.5}$,[16] or $RE'_{5-x}RE''_xSi_4$ (RE' and RE'' denote different metals).[17,18]

Our continued interest in the structure−property relationships in various rare-earth metal germanides was steered toward the remarkable properties of the materials with the above-named types after the mixed-valent $Yb_{5-x}Mg_xGe_4$ compound ($x \approx 1.0-1.2$) with the Gd_5Si_4 type structure was synthesized and structurally characterized.[11] Although formally a solid-solution, the structure of $Yb_{5-x}Mg_xGe_4$ exhibits coloring of the cation sites, that is, Mg−Yb substitutions take place on specific crystallographic positions. This finding captured our attention as it could potentially offer the control sought after in designed syntheses and could provide a viable tool for the purposeful tuning of physical properties. Hence, we set out to investigate the crystal chemistry and magnetic properties of the other substitution derivatives of the rare-earth metal germanides with the same structure. Through these efforts, we synthesized a series of new solid solutions $RE_{5-x}Mg_xGe_4$, which exist for limited homogeneity ranges ($x \approx 1.0-2.3$) and form with the mid-to-late rare-earth metals (RE = Gd−Tm, Lu), as well as Y. Their structures were determined by single-crystal X-ray diffraction and are at the focus of this article. Temperature and field dependent direct current (*dc*) magnetic susceptibility measurements are also discussed, revealing complex magnetic structures at low temperatures.

Experimental Section

Synthesis. The synthetic efforts were modeled after the previously described $La_{5-x}Ca_xGe_4$ ($x \approx 3.0-3.5$),[10] and $Yb_{5-x}Mg_xGe_4$ ($x \approx 1.0-1.2$).[11] A variety of reaction conditions were investigated and are described in detail in the Supporting Information section. Here, we only call attention to the fact that because of the high vapor pressure of Mg metal (bp 1363 K),[19] reactions in open crucibles (heated under vacuum or under inert gas flow) were not deemed appropriate. For the same reason, arc-melting of the pure elements was also never attempted. Instead, all high temperature experiments were carried out in sealed Nb-tubes, and they were cautiously designed and monitored as a safety precaution.[20]

The high melting points of the rare-earth metals and the corresponding RE_5Ge_4 binary phases,[21] together with the low boiling point of Mg proved a challenging synthetic problem. It imposed limits on the accessible temperatures, thus, precluding the high-yield synthesis of a wider range of $RE_{5-x}Mg_xGe_4$ (RE = Gd−Tm, Lu, and Y) phases. We also point out that other studies involving the rare-earth metals and Mg, particularly in the cases of the closely related RE_2MgGe_2,[22] have also come across a similar problem. To circumvent it, a synthetic route using Mg_2Ge as a precursor [22a] or quick induction melting at very high temperatures [22b] have been suggested as alternatives. While these approaches may have been successfully applied toward the synthesis of the latter compounds, the results from our investigations suggest that the RE_5Ge_3, REGe, and Mg_2Ge binaries, [23] as well as the RE_2MgGe_2 ternary phases,[22] are the most recurring side-products. This likely indicates that under the given experimental conditions, the $RE_{5-x}Mg_xGe_4$ (RE = Gd−Tm, Lu, and Y) phases are unstable with respect to the neighboring simpler compounds in the corresponding phase diagrams.

Powder X-ray Diffraction. X-ray powder diffraction patterns were taken at room temperature using a Rigaku Miniflex powder diffractometer (Cu Kα radiation, 2θ range from 10 to 80° with a step size of 0.05 and 5 s/step counting time). The collected powder patterns were primarily used for phase identification of the reaction products. Such analyses were carried out using the JADE 6.5 software package. According to the powder X-ray diffraction data, polycrystalline samples from all $RE_{5-x}Mg_xGe_4$ (RE = Gd−Tm, Lu, and Y) phases are stable in air for months.

(14) For instance, following the Zintl-Klemm concept (Kauzlarich, S. M.; *Chemistry, Structure and Bonding of Zintl Phases and Ions*; VCH Publishers: New York, 1996; and references therein), the 31 valence electrons in the RE_5Ge_4 formula unit, depending on the structure and the number of Ge−Ge bonds can be counted as follows: $[RE^{3+}]_5[Ge_2^{6-}]_2[3e^-]$ (all Ge atoms are dimerized, Gd_5Si_4 type) or as $[RE^{3+}]_5[Ge_2^{6-}][Ge^{4-}]_2[1e^-]$ (only a half of the Ge atoms are dimerized, Sm_5Ge_4 type), respectively.

(15) (a) Mozharivskyj, Y.; Tsokol, A. O.; Miller, G. J. *Z. Kristallogr.* **2006**, *221*, 493. (b) Wang, H. B.; Altounian, Z.; Ryan, D. H. *Phys. Rev. B* **2002**, *66*, 214413.

(16) Zhang, T.; Chen, Y.; Tang, Y.; Tu, M. *J. Alloys Compd.* **2006**, *422*, 25.

(17) Elbicki, J. M.; Zhang, L. Y.; Obermyer, R. T.; Wallace, W. E.; Sankar, S. G. *J. Appl. Phys.* **1991**, *69*, 5571.

(18) (a) Pecharsky, V. K.; Gschneidner, K. A.Jr. *Pure Appl. Chem.* **2007**, *79*, 1383. (b) Shimotomai, S.; Ido, H. *J. Appl. Phys.* **2006**, *99*, 08Q109. (c) Spichkin, Y. I.; Pecharsky, V. K.; Gschneidner, K. A.Jr. *J. Appl. Phys.* **2001**, *89*, 1738. (d) Rodewald, U. Ch.; Heying, B.; Johrendt, D.; Hoffmann, R.-D.; Pöttgen, R. *Z. Naturforsch.* **2004**, *59b*, 174. (e) Singh, N. K.; Pecharsky, V. K.; Gschneidner, K. A.Jr. *Phys. Rev. B* **2008**, *77*, 054414.

(19) *CRC Handbook of Chemistry and Physics*, 83rd ed.; CRC Press LLC: Boca Raton, FL, 2002.

(20) *Caution!* Such reactions in sealed Nb-tubes can lead to a high-pressure, and may result in a leak of Mg and its subsequent reaction with walls of the fused silica ampoules. To minimize the negative effects of such leaks, the silica ampoules should be made sufficiently long, so that one of their ends is left protruding outside the furnace, should leaks occur (for a condensation). If this is not possible because of furnace design or other practical considerations, the Nb-containers should be double-jacketed and sealed within two fused silica tubes.

(21) Massalski, T. B. *Binary Alloy Phase Diagrams*; American Society for Metals: Materials Park, OH, 1990.

(22) (a) Choe, W.; Miller, G.; Levin, E. *J. Alloys Compd.* **2001**, *329*, 121. (b) Kraft, R.; Pöttgen, R. *Montash. Chem.* **2004**, *135*, 1327.

(23) Villars, P.; Calvert, L. D. *Pearson's Handbook of Crystallographic Data for Intermetallic Phases*, 2nd ed.; American Society for Metals: Materials Park, OH, 1991.

Table 1. Selected Crystallographic Data for a Series of $Ho_{5-x}Mg_xGe_4$ Samples ($1.23 \leq x \leq 2.08$)

empirical formula	$Ho_{2.92(1)}Mg_{2.08}Ge_4$	$Ho_{3.05(1)}Mg_{1.95}Ge_4$	$Ho_{3.20(1)}Mg_{1.80}Ge_4$	$Ho_{3.29(1)}Mg_{1.71}Ge_4$	$Ho_{3.62(1)}Mg_{1.38}Ge_4$	$Ho_{3.77(1)}Mg_{1.23}Ge_4$
formula weight	822.17	840.80	861.54	874.20	920.25	942.40
space group				*Pnma* (No. 62)		
λ, Å				0.71073		
T, K				120		
a, Å	6.9989(12)	7.0084(7)	7.0260(13)	7.033(4)	7.0710(11)	7.0845(13)
b, Å	14.265(2)	14.2769(14)	14.315(3)	14.337(9)	14.419(2)	14.445(3)
c, Å	7.6438(13)	7.6482(7)	7.6609(14)	7.661(5)	7.6627(12)	7.6677(14)
V, Å^3, $Z = 4$	763.1(2)	765.27(13)	770.5(2)	772.5(8)	781.2(2)	784.7(2)
c/a	1.092	1.091	1.090	1.089	1.084	1.082
ρ_{calcd}, g cm^{-3}	7.156	7.298	7.427	7.517	7.824	7.977
μ (Mo Kα), cm^{-1}	454.7	466.9	478.5	486.3	513.2	526.5
R_1 [$I > 2\sigma(I)$] [a]	0.0168	0.0199	0.0337	0.0213	0.0327	0.0319
wR_2 [$I > 2\sigma(I)$] [a]	0.0375	0.0398	0.0632	0.0468	0.0532	0.0586
R_1 [all data] [a]	0.0187	0.0220	0.0552	0.0263	0.0457	0.0468
wR_2 [all data] [a]	0.0383	0.0404	0.0690	0.0486	0.0576	0.0621

[a] $R_1 = \sum||F_o| - |F_c||/\sum|F_o|$; $wR_2 = [\sum w(F_o^2 - F_c^2)^2/\sum w(F_o^2)^2]^{1/2}$, where $w = 1/[\sigma^2F_o^2 + (A\cdot P)^2 + B\cdot P]$, $P = (F_o^2 + 2F_c^2)/3$; A and B are weight coefficients. For additional information, please see the CIF file in the Supporting Information.

Table 2. Selected Crystallographic Data for $RE_{5-x}Mg_xGe_4$ (RE = Gd, Tb, Dy, Er, Tm, Lu, and Y)

empirical formula	$Gd_{3.55(1)}Mg_{1.45}Ge_4$	$Tb_{3.52(1)}Mg_{1.48}Ge_4$	$Dy_{3.50(1)}Mg_{1.50}Ge_4$	$Er_{3.41(1)}Mg_{1.59}Ge_4$	$Tm_{3.51(1)}Mg_{1.49}Ge_4$	$Lu_{3.60(1)}Mg_{1.40}Ge_4$	$Y_{3.49(1)}Mg_{1.51}Ge_4$
formula weight	883.51	886.07	895.23	899.37	919.89	954.29	637.53
space group				*Pnma* (No. 62)			
λ, Å				0.71073			
T, K				120			
a, Å	7.1574(9)	7.128(5)	7.0845(14)	7.0214(5)	7.0128(9)	6.9750(8)	7.085(2)
b, Å	14.623(2)	14.512(11)	14.425(3)	14.3063(10)	14.270(2)	14.224(2)	14.465(4)
c, Å	7.7801(9)	7.732(6)	7.687(2)	7.6350(5)	7.5998(9)	7.5619(9)	7.718(2)
V, Å^3, $Z = 4$	814.3(2)	799.8(10)	785.6(3)	766.94(9)	760.5(2)	750.2(2)	791.1(4)
c/a	1.087	1.085	1.085	1.087	1.084	1.084	1.087
ρ_{calcd}, g cm^{-3}	7.207	7.358	7.569	7.789	8.034	8.449	5.266
μ (Mo Kα), cm^{-1}	430.3	455.4	479.2	523.5	561.2	626.9	391.6
R_1 [$I > 2\sigma(I)$] [a]	0.0323	0.0293	0.0366	0.0215	0.0282	0.0249	0.0172
wR_2 [$I > 2\sigma(I)$] [a]	0.0658	0.0614	0.0582	0.0445	0.0526	0.0492	0.0387
R_1 [all data] [a]	0.0476	0.0368	0.0593	0.0272	0.0313	0.0339	0.0194
wR_2 [all data] [a]	0.0697	0.0648	0.0661	0.0460	0.0553	0.0517	0.0395

[a] $R_1 = \sum||F_o| - |F_c||/\sum|F_o|$; $wR_2 = [\sum w(F_o^2 - F_c^2)^2/\sum w(F_o^2)^2]^{1/2}$, where $w = 1/[\sigma^2F_o^2 + (A\cdot P)^2 + B\cdot P]$, $P = (F_o^2 + 2F_c^2)/3$; A and B are weight coefficients. For additional information, please see the CIF file in the Supporting Information.

For the samples for which magnetization measurements were completed, the purity of the material was ensured by qualitative peak-profile fits of the powder patterns. These were done employing the GSAS code (taking the atomic coordinates, occupancies, and temperature factors from the single-crystal refinements). A representative plot showing the calculated and the observed intensities, together with the difference curve is provided as Supporting Information.

Single Crystal X-ray Diffraction. Data collections were carried out on a Bruker SMART CCD diffractometer with a 3-circle goniometer. Full spheres of single-crystal diffraction data were gathered for a multitude of crystals (approximately 30) from different reactions. In all cases, crystals were chosen under a microscope, cut to suitable dimensions for data collection (ca. 50 μm), and mounted on glass fibers with Paratone-N oil. All data acquisitions were done in four batches with a scan width of 0.4° in ω and 10−15 s exposure time per frame. The SMART software was used to manage the data collections, examine the crystal quality, and obtain the orientation matrices (based on several hundred indexed reflections from all frames). Data reduction and integration and global cell constants refinements were done using SAINTplus. Semiempirical absorption correction based on equivalent reflections was applied with the aid of SADABS. The subsequent processing of the data was straightforward—the reflection conditions and the intensity statistics clearly suggested the space group *Pnma* (No. 62), which together with the similarities of the cell parameters with those of the known RE_5Ge_4 compounds,[24] provided for the quick "structure solutions". Hence, for the initial refinements, the known atomic coordinates and labeling scheme were used. Following that, the structures were successfully refined to convergence with the aid of SHELXL (see Results and Discussion for specific details pertaining to the RE/Mg site preferences and subtle differences in the structures of RE_5Ge_4 and $RE_{5-x}Mg_xGe_4$).

Because of the very large number of refined structures and the difficulty of representing the data associated with all of them, we have chosen to focus the attention on the $Ho_{5-x}Mg_xGe_4$ ($1.23 \leq x \leq 2.08$) samples. These were selected as representative cases for the following reasons: (i) Ho is nearly in the middle of the studied series of rare earth metals and (ii) the six $Ho_{5-x}Mg_xGe_4$ ($1.23 \leq x \leq 2.08$) specimens describe a wide homogeneity range, likely close to its entirety. Important data collection and structure refinements parameters for all $Ho_{5-x}Mg_xGe_4$ crystals are given in Table 1. Table 2 lists relevant crystallographic data for seven $RE_{5-x}Mg_xGe_4$ analogues (RE = Gd, Tb, Dy, Er, Tm, Lu, and Y). Further structural information for the remaining $RE_{5-x}Mg_xGe_4$, as well as for the binary Ho_5Ge_4 (for consistency, also refined from single-crystal data at the same temperature) is provided as Supporting Information. The crystallographic information files (CIF) from all data collections are also furnished in the Supporting Information section. They

(24) Smith, G. S.; Tharp, A. G.; Johnson, Q. *Acta Crystallogr.* **1967**, *22*, 940.

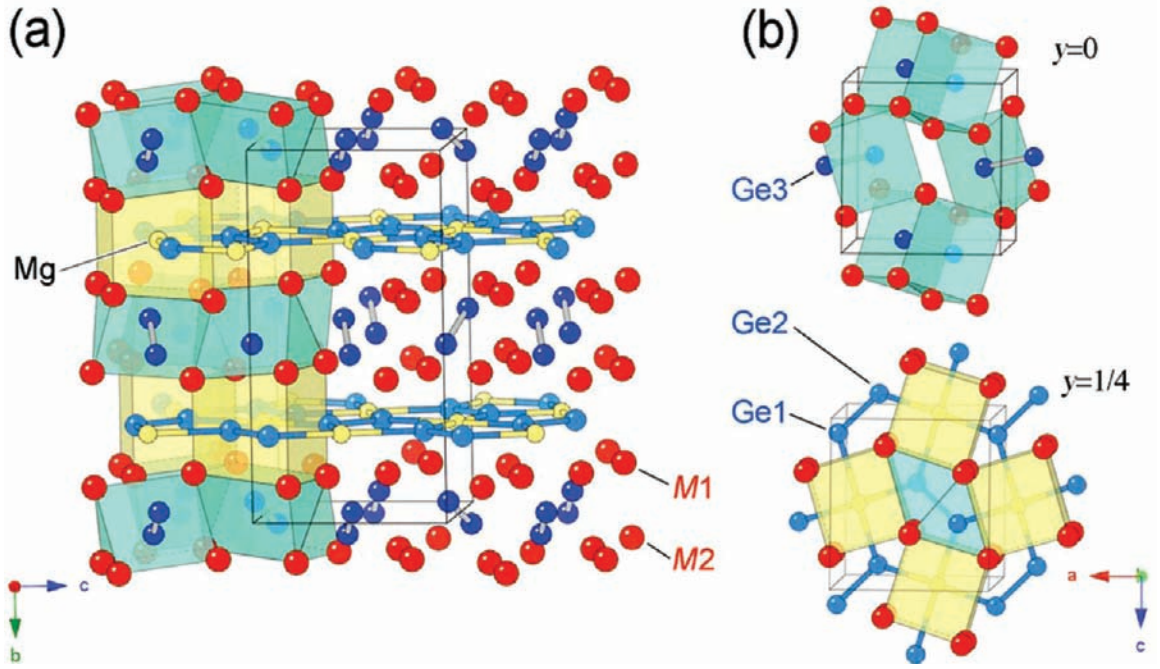

Figure 1. (a) Off [100]-view of the crystal structure of the $RE_{5-x}Mg_xGe_4$ (RE = Gd−Tm, Lu and Y) compounds emphasizing the Ge_2 dimers and the packing of the rare-earth metal polyhedra. The unit cell is outlined. The slabs in light-blue also represent the Ho_2MgGe_2-like fragments (Mo_2FeB_2 type) and the slabs in yellow represent HoGe-like fragment (FeB type), respectively, allowing the structure to be rationalized as their intergrowth. (b) Close-up views of the two layers, viewed approximately down the *b*-axis.

have been deposited with Fachinformationszentrum Karlsruhe, 76344 Eggenstein-Leopoldshafen, Germany, (fax: (49) 7247−808−666; e-mail: crysdata@fiz.karlsruhe.de) with depository numbers: CSD-420265 ($Ho_{2.92(1)}Mg_{2.08}Ge_4$), CSD-420266 ($Ho_{3.05(1)}Mg_{1.95}Ge_4$), CSD-420267 ($Ho_{3.20(1)}Mg_{1.80}Ge_4$), CSD-420269 ($Ho_{3.29(1)}Mg_{1.71}Ge_4$), CSD-420268 ($Ho_{3.62(1)}Mg_{1.38}Ge_4$), CSD-420270 ($Ho_{3.77(1)}Mg_{1.23}Ge_4$), CSD-420271 ($Gd_{3.55(1)}Mg_{1.45}Ge_4$), CSD-420272 ($Tb_{3.52(1)}Mg_{1.48}Ge_4$), CSD-420273 ($Dy_{3.50(1)}Mg_{1.50}Ge_4$), CSD-420274 ($Er_{3.41(1)}Mg_{1.59}Ge_4$), CSD-420277 ($Tm_{3.51(1)}Mg_{1.49}Ge_4$), CSD-420275 ($Lu_{3.60(1)}Mg_{1.40}Ge_4$), CSD-420278 ($Y_{3.49(1)}Mg_{1.51}Ge_4$), CSD-420276 ($Ho_5Ge_4$).

Magnetization Measurements. Field cooled (FC) and zero field cooled (ZFC) *dc* magnetization (M) measurements were completed using a Quantum Design MPMS SQUID magnetometer in the temperature range 5−300 K and in an applied field (H) of 100 Oe. The samples were secured in a custom-designed low background holder; the raw magnetization data were corrected for the holder contribution and converted to molar susceptibility ($\chi_m = M/H$). For one of them, $Ho_{3.05(1)}Mg_{1.95}Ge_4$, a phase-pure sample with a very close match between a nominal and refined composition, field dependent measurements at low temperatures and in applied fields up to 50 kOe were also completed.

Results and Discussion

Structure and Bonding. Structure Description. The metal-rich $RE_{5-x}Mg_xGe_4$ compounds ($x \approx 1.0-2.3$; RE = Gd−Tm, Lu, Y), as their formula suggests, are substitution derivatives of the RE_5Ge_4 binary phases (6 crystallographically unique atoms in the asymmetric unit, Pearson's code *oP*36).[23−25] Their structure (Figure 1) can be described as being built from two separate fragments of the rare-earth metals (disregarding the RE/Mg mixing): slabs of condensed trigonal prisms (light blue) and slabs of trigonal prisms fused within parallelepipeds (yellow). All prisms are centered by Ge atoms, while all "cubes" are centered by Mg atoms. Both slabs run parallel to the *ac*-plane and are stacked in an alternating $ABA'B'$ manner along the direction of the *b* crystallographic axis. Alternatively, using the ideas discussed for Yb_4MgGe_4,[11] the structure can also be rationalized as an intergrowth of RE_2MgGe_2 (Mo_2FeB_2 type [22,23]) and REGe (FeB type [23]) fragments, a formalism that can be extended in this case as well. In this view, the Mg atom occupying the Wyckoff site 4*c* (Table 3) can be considered as centering a distorted octahedron of Ge atoms, which is inscribed within a cube of rare-earth metal atoms. Similar "coloring" of the metal sites has also been established for the Y-substituted $Gd_{5-x}Y_xSi_4$.[12]

Since many recent reports have already discussed the structures,[1−13] herein we only provide a brief account. The discussion is focused on the variations of the metrics of the structures as a function of the Mg-content and the observed cation site preferences. These considerations are illustrated in the next paragraphs on the example of $Ho_{3.05(1)}Mg_{1.95}Ge_4$ (for brevity, $Ho_3Mg_2Ge_4$ hereafter).

Table 3. Atomic Coordinates and Equivalent Isotropic Displacement Parameters (U_{eq})[a] for $Ho_{3.05(1)}Mg_{1.95}Ge_4$

atom	site	x	y	z	U_{eq} (Å^2)
Mg	4*c*	0.3412(5)	1/4	0.0116(4)	0.0090(7)
*M*1 [b]	8*d*	0.1700(1)	0.1263(1)	0.3220(1)	0.0050(2)
*M*2 [c]	8*d*	0.0066(1)	0.0949(1)	0.8169(1)	0.0055(2)
Ge1	4*c*	0.9728(1)	1/4	0.0971(1)	0.0073(2)
Ge2	4*c*	0.2130(1)	1/4	0.6380(1)	0.0047(2)
Ge3	8*d*	0.1687(1)	0.9631(1)	0.5341(1)	0.0054(2)

[a] U_{eq} is defined as one-third of the trace of the orthogonalized U_{ij} tensor. [b] Refined as a statistical mixture of Ho and Mg in a ratio 52.6:47.4. [c] Refined as 100% Ho.

(25) Iglesias, J. E.; Steinfink, H. *J. Less-Common Met.* **1972**, *26*, 45.

Table 4. Important Bond Distances (Å) in $Ho_{3.05(1)}Mg_{1.95}Ge_4$

atom pair		distance (Å)	atom pair		distance (Å)
Ge1—	Ge2	2.563(1)	Mg—	*M*1 (×2)	3.241(2)
	Mg	2.710(3)		*M*1 (×2)	3.327(2)
	*M*1 (×2)	2.8188(8)		*M*2 (×2)	3.420(2)
	*M*1 (×2)	2.8220(8)		*M*2 (×2)	3.481(2)
	*M*2 (×2)	3.0955(7)	*M*1—	*M*1	3.533(1)
	Ge1	3.279(3)		*M*2	3.5550(7)
Ge2—	Ge1	2.563(1)		*M*2	3.6600(6)
	Mg	2.780(3)		*M*1 (×2)	3.6729(4)
	Mg	2.834(3)		*M*2	3.8876(7)
	*M*2	2.9741(6)		*M*2	3.9804(7)
	*M*1	3.0073(8)		*M*2	4.0532(7)
	Ho2 (×2)	3.0351(7)	*M*2—	*M*1	3.5550(7)
Ge3—	Ge3	2.640(1)		*M*2 (×2)	3.6507(4)
	*M*1	2.7790(8)		*M*1	3.6600(6)
	*M*1	2.8382(8)		*M*1	3.8876(7)
	*M*1	2.9069(8)		*M*2	3.8988(7)
	*M*2	2.9381(7)		*M*1	3.9804(7)
	Mg	3.0580(8)		*M*1	4.0532(7)
	*M*2	3.0631(7)			
	*M*2	3.0838(7)			

The refined atomic coordinates, equivalent isotropic displacement parameters, and selected interatomic distances for $Ho_3Mg_2Ge_4$ are provided in Tables 3 and 4, respectively. Details concerning the remaining Ho-members and all other rare-earth metal analogues can be found in the Supporting Information.

Unit Cell Parameters. Formally, $Ho_3Mg_2Ge_4$ crystallizes with the Gd_5Si_4 type structure,[25] which is a notable difference with the "parent" Ho_5Ge_4—the latter is assigned to the Sm_5Ge_4 structure.[23,24] Although both have the same space group and very similar atomic coordinates, an important difference in their bonding characteristics needs to be specifically pointed out. Put simply, the two structures have different fractions of the Ge atoms that form Ge−Ge bonds, all in the Gd_5Si_4 structure and half in the Sm_5Ge_4 structure.[14] A widely used indicator for differentiating between the two is the c/a ratio,[5] which typically is on the order or greater than 1.05 for the former and close to 1.00 for the latter.[26] Along these lines, the unusual, more than 6% difference between the a-axis of Ho_5Ge_4 (a = 7.567(3) Å)[27] and the a-axis of $Ho_3Mg_2Ge_4$ (a = 7.0084(7) Å) must be noted. For comparison, the b-axis changes from 14.562(7) Å for Ho_5Ge_4 to 14.2769 (14) Å for $Ho_3Mg_2Ge_4$, respectively. Such contraction in directions of a and b is accompanied by a small elongation of the c-axis, from 7.638(4) Å to 7.6482(7) Å. The net effect is that the c/a ratio increases sharply from 1.009 for Ho_5Ge_4 to c/a = 1.091 for $Ho_3Mg_2Ge_4$, indicative of the transformation from the Sm_5Ge_4 to the Gd_5Si_4 type structure. Similar effect is also noted for the remaining $RE_{5-x}Mg_xGe_4$ (RE = Gd, Tb, Dy, Er, Tm, Lu and Y) phases (see Table 2).

The increased Mg content correlates well with the monotonic decrease in the lattice parameters, as shown in Table 1 (owing to the slightly smaller size of Mg^{2+} (0.86 Å) compared to that of Ho^{3+} (1.04 Å).[28] However, the unit cell contraction is not isotropic—with increasing the amount of Ho being substituted by Mg, the c- and a-axes contract by as little as 0.4% and 1.1%, respectively, while the b-axis gets smaller by nearly 1.4%. Regardless of that, the c/a ratio remains nearly constant: c/a increases slightly from 1.082 for $Ho_{3.77(1)}Mg_{1.23}Ge_4$ to c/a = 1.092 for $Ho_{2.92(1)}Mg_{2.08}Ge_4$. The same dependence is seen for all other synthesized samples. Among them, $Dy_{2.74(2)}Mg_{2.25}Ge_4$ is Mg-richest and has c/a ratio of 1.094 and $Er_{4.05(5)}Mg_{0.95}Ge_4$, which is Mg-leanest, has c/a ratio of 1.070. This indicates that no crystallographic transitions occur as almost 45% at. of the rare-earth metal is replaced with Mg.

Ge−Ge Distances. All Ge atoms in the $Ho_3Mg_2Ge_4$ structure are dimerized (formally $[Ge_2]^{6-}$, isoelectronic with the Br_2 molecule). The importance of the Ge−Ge bonds to the properties had been discussed at length in earlier publications,[2−5] we just recall a distinction between the two kinds of Ge dimers: the ones within the HoGe fragment are formed by two symmetry-related Ge atoms, (Ge3, Table 3), while the ones within the imaginary Ho_2MgGe_2 slab are formed between the atoms labeled as Ge1 and Ge2, respectively. As can be seen from the distances presented in Table 4, the Ge1−Ge2 dimers are shorter than the Ge3−Ge3 ones, 2.563(1) Å versus 2.640(1) Å. Both values are well within the range for Ge−Ge distances reported for many other binary and ternary rare-earth metal germanides,[22,29−32] as well as the isostructural $RE_{5-x}Ca_xGe_4$ (RE = La, Ce),[10] and $RE_{5-x}Mg_xGe_4$ analogues (RE = Gd, Tb, Dy, Er, Tm, Lu and Y). For the latter, the Ge1−Ge2 distances measure 2.52−2.58 Å across the series, whereas the Ge3−Ge3 distances are on the order of 2.64−2.70 Å (Supporting Information, Tables S4−S13). For comparison, the Ge1−Ge2 dimers in Ho_5Ge_4 are much longer, measuring 2.707(3) Å, while the Ge3−Ge3 contacts are about 3.59 Å long (Supporting Information, Table S3). These variations of the Ge−Ge distances, as alluded to already, correlate with the Mg content and the overall electron count and are elaborated on next.

(26) The c/a ratio can also be used to evaluate structural trends, particularly changes in the number of Ge−Ge bonds upon heating/cooling or the application of external field. Large variations indicate that there is "making and/or breaking" of Ge−Ge bonds, as seen in $Gd_5(Si_xGe_{1-x})_4$ for example.[5]

(27) For greatest accuracy, we compare the cell parameters for $Ho_3Mg_2Ge_4$ and Ho_5Ge_4, both obtained from our own single-crystal X-ray diffraction work at 120 K (Supporting Information, Tables S1, S2, and S3).

(28) Shannon, R. D. *Acta Crystallogr.* **1976**, *A 32*, 751.

(29) (a) Schobinger-Papamantellos, P. *J. Chem. Phys. Solids* **1978**, *39*, 197. (b) Schobinger-Papamantellos, P.; Niggli, A. *J. Phys. (Paris)* **1979**, *40*, 156.

(30) Salamakha, P. S.; Sologub, O. L.; Bodak, O. I. Ternary Rare-Earth-Germanium Systems. In *Handbook on the Physics and Chemistry of Rare Earths*; Gschneidner, K. A., Jr., Eyring, L., Eds.; North Holland: Amsterdam, 1999; Vol. *27*, p 1.

(31) (a) Tobash, P. H.; Lins, D.; Bobev, S.; Lima, A.; Hundley, M. F.; Thompson, J. D.; Sarrao, J. L. *Chem. Mater.* **2005**, *17*, 5567. (b) Tobash, P. H.; Lins, D.; Bobev, S.; Hur, N.; Thompson, J. D.; Sarrao, J. L. *Inorg. Chem.* **2006**, *45*, 7286. (c) Bobev, S.; Bauer, E. D.; Thompson, J. D.; Sarrao, J. L.; Miller, G. J.; Eck, B.; Dronskowski, R. *J. Solid State Chem.* **2004**, *177*, 3545. (d) Tobash, P. H.; Meyers, J. J.; DiFilippo, G.; Bobev, S.; Ronning, F.; Thompson, J. D.; Sarrao, J. L. *Chem. Mater.* **2008**, *20*, 2151. (e) Tobash, P. H.; Bobev, S. *J. Solid State Chem.* **2007**, *180*, 1575. (f) Bobev, S.; Bauer, E. D. *Acta Crystallogr.* **2005**, *E61*, i73. (g) Tobash, P. H.; DiFilippo, G.; Bobev, S.; Hur, N.; Thompson, J. D.; Sarrao, J. L. *Inorg. Chem.* **2007**, *46*, 8690.

(32) (a) Mao, J.-G.; Goodey, J.; Guloy, A. M. *Inorg. Chem.* **2002**, *41*, 931. (b) Pöttgen, R.; Simon, A. *Z. Anorg. Allg. Chem.* **1996**, *622*, 779. (c) Guloy, A.; Corbett, J. D. *J. Solid State Chem.* **2005**, *178*, 1112. (d) Schobinger-Papamantellos, P.; Buschow, K. H. J. *J. Less-Common Met.* **1989**, *146*, 279. (e) Salvador, J. R.; Bilc, D.; Mahanti, S. D.; Hogan, T.; Guo, F.; Kanatzidis, M. G. *J. Am. Chem. Soc.* **2004**, *126*, 4474. (f) Johrendt, D.; Mewis, A.; Drescher, K.; Wasser, S.; Michels, G. *Z. Anorg. Allg. Chem.* **1996**, *622*, 589.

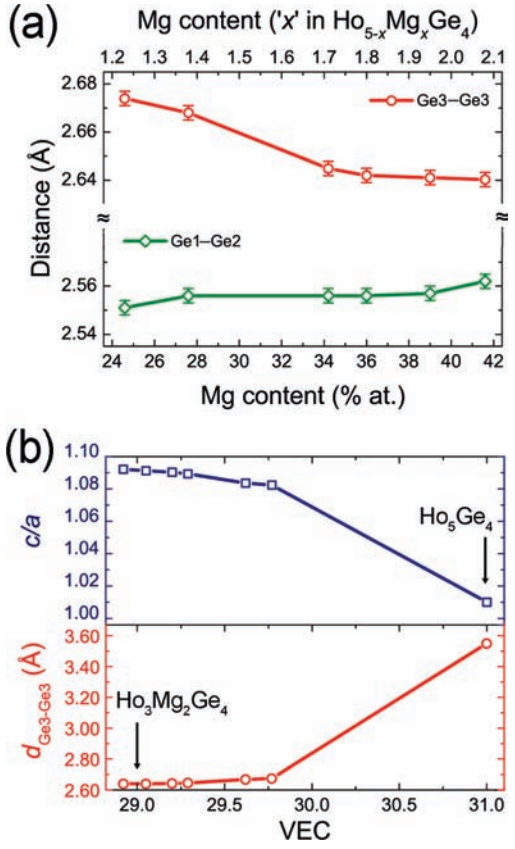

Figure 2. (a) Variations of the Ge−Ge distances in the two different Ge_2 dimers in the structure of the $Ho_{5-x}Mg_xGe_4$ ($1.23 \le x \le 2.08$) compounds as a function of the Mg content. (b) Side-by-side comparison of the dependence of the Ge3−Ge3 distances and the c/a ratio in the structure of Ho_5Ge_4 and the Mg-substituted variants $Ho_{5-x}Mg_xGe_4$ ($1.23 \le x \le 2.08$) as a function of the valence electron concentration (per formula unit).

The subtle dependence of the two types of Ge−Ge distances in the series $Ho_{5-x}Mg_xGe_4$ ($1.23 \le x \le 2.08$) as a function of "x" is plotted in Figure 2a. From the graph, it is evident that a gradual decrease in the Ge3−Ge3 separation (ca. 1.5%), that is, strengthening of the bond is concomitant to the Mg content being increased. A reverse dependence is seen for the Ge1−Ge2 bonds: they are only slightly (ca. 0.3%) elongated, that is, somewhat weakened when "x" increases. Another way to look at this trend is illustrated in Figure 2b, where the Ge3−Ge3 distances and the c/a ratios are plotted as a function of the valence electron concentration per formula unit (VEC). The plot clearly shows that the Ge-atoms come closer together when the VEC decreases, that is, they are being oxidized, and vice versa—they are further apart when being reduced, that is, the VEC increases. Although the contribution of the crystal packing cannot be disregarded, the above dependence is arguably indicative of an electronic effect at play. The total number of valence electrons decreases as the trivalent Ho is substituted by the nominally divalent Mg, thereby leading to an electron count that is closer to the 28 e^- per f.u., expected from the Zintl−Klemm rules.[14] Recent computational studies corroborate the idea that while the structure might be able to accommodate slightly higher or lower than optimal number of valence electrons,[10] the decrease of the number of electrons in conduction bands will reinforce Ge3−Ge3 bonds with little effect on the Ge1−Ge2 bonds. Such an unique feature of this structure, makes it a "continuous tuning knob", as demonstrated previously for $Gd_5(Si_xGe_{1-x})_4$,[5] $Gd_5(Ga_xGe_{1-x})_4$,[9] and now for $RE_{5-x}Mg_xGe_4$.

Site Preferences. As was the case for Yb_4MgGe_4,[11] single-crystal refinements readily confirmed a "coloring" of the metal substructure; from the three available cation sites, the one with Wyckoff index 4*c* is exclusively occupied by Mg (Table 3). Such experimental finding follows the computational analysis of Misra and Miller,[12] which indicates that the 4*c* site should be occupied by the metal with the higher ionization energy: Mg in $Ho_3Mg_2Ge_4$. This consideration is based on electronic arguments and is in excellent agreement with the distribution expected from simple geometric reasoning as well—being more "tightly" coordinated to neighboring Ge atoms (Table 4), the 4*c* site should be taken by the smaller cations, Y^{3+} and Mg^{2+}, respectively.

Out of the remaining two 8*d* sites, the position labeled *M*1 was refined as a statistical mixture of the rare-earth metal and magnesium; the scattering power of the atom assigned to this site was consistent with about 48% at. Mg substitution (for $Ho_3Mg_2Ge_4$). The third cation site, labeled as *M*2, always refined with the scattering factor of a fully occupied Ho atom, and its site occupancy never deviated from full (within 3σ), suggesting that this crystallographic position is not susceptible to mixing with Mg (at least not until *M*1 is fully substituted by Mg). This point is manifested by comparing the refinements for the Mg-richest phase $Ho_{2.92(1)}Mg_{2.08}Ge_4$, where the *M*1 site was refined as a 45.9: 54.1 mixture of Ho and Mg, while for the most Mg-lean $Ho_{3.77(1)}Mg_{1.23}Ge_4$, the *M*1 site was refined as a 88.6 : 11.4 mixture of Ho and Mg (see the Supporting Information, Tables S4−S13). In both cases, the *M*2 site is fully occupied by Ho. The refined occupancies for the *M*1 and *M*2 sites in all other $RE_{5-x}Mg_xGe_4$ phases (*RE* = Gd−Dy, Er−Tm, Lu, Y) are in the same range as well (see the Supporting Information, Tables S14−S27). With that regard, we draw attention to the fact that because of the great difference in the atomic numbers, the scattering factors for Mg and the rare-earth metals are quite different, which allows for an excellent "X-ray contrast". This, combined with the high-quality data (with data-to-parameter ratio greater than 17) provides for crystallographic refinements with a very high statistical significance.

Periodic Trends. On the basis of the conducted numerous syntheses, it seems reasonable to conclude that the $RE_{5-x}Mg_xGe_4$ (*RE* = Gd−Tm, Lu, and Y) family extends only over the mid-to-late rare-earth metals. All attempts to broaden the series to the early rare-earth metals (*RE* = La−Nd, Sm) were unsuccessful (see Supporting Information). These findings may seem puzzling, given that both the end members RE_5Ge_4 (*RE* = La−Nd, Sm) and the Ca-substituted $RE_{5-x}Ca_xGe_4$ (*RE* = La, Ce) variants,[10] are known with the same structure. This can be explained taking into consideration the fact that the ionic radii of the early lanthanide cations (La^{3+}/r = 1.17 Å; Ce^{3+}/r = 1.15 Å; Pr^{3+}/r = 1.13 Å; Nd^{3+}/r = 1.12 Å) and that of Ca^{2+} (Ca^{2+}/r = 1.14 Å) are matching very well, while the late lanthanide cations are smaller (with radii varying from 1.00 to 1.08 Å).[28] Evidently, for this atomic arrangement, an optimal packing efficiency cannot be achieved when the large La is substituted with the

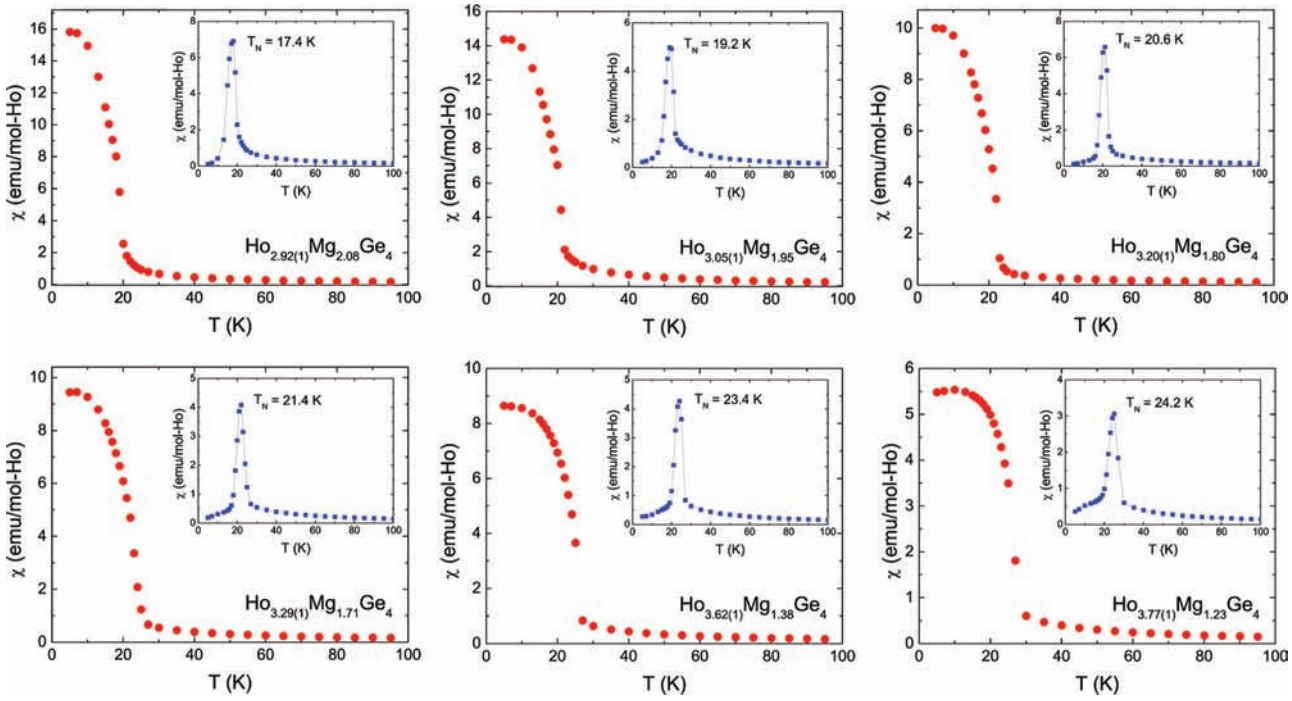

Figure 3. Magnetic susceptibility ($\chi = M/H$) vs temperature for the series $Ho_{5-x}Mg_xGe_4$ ($1.23 \leq x \leq 2.08$). Data are normalized per mol-Ho with field cooled (FC) measurements presented in the main panels and zero field cooled (ZFC) measurements presented in the insets. The corresponding Néel temperatures (T_N) from the ZFC plots are marked down. All measurements were completed in applied field of 100 Oe.

much smaller Mg, but can be accomplished when the more comparable in size Ca is used.[10]

Even though fulfillment of the electronic requirements is not the only factor of importance for the realization of this structure, the electron counting arguments can also be used to explain (qualitatively) the propensity of the RE_5Ge_4 compounds to be "doped" with Mg or Ca. Take for example the unknown Ca_5Ge_4, which would be formally electron-deficient, and the known La_5Ge_4, which is electron-rich[10,14]—forming an intergrowth between the two would strengthen all interactions in the structure and should be thermodynamically favored. Depending on the specific atomic arrangement, that is, whether all Ge atoms are dimerized or not, the optimal number of trivalent rare-earth metal atoms to be replaced with electron poorer Ca or Mg will be 3 per formula unit (Gd_5Si_4 type, all dimers), or 1 per formula unit (Sm_5Ge_4 type, normal and "broken" dimers).[14] These considerations are substantiated by density functional theory (DFT) calculations by Seo et al.,[10] and by the observed dependence of the Ge3−Ge3 bonds on the VEC, discussed above. Following the same reasoning, we can also speculate that the homogeneity range in $RE_{5-x}Mg_xGe_4$ can possibly be increased higher than the presently attained 40−45% at. Mg. This conjecture can be inferred from the above-mentioned formal electron count (one electron higher than the ideal 28 e^- per f.u.[14]), as well as the earlier reports on Ca-substituted $RE_{5-x}Ca_xGe_4$ (RE = La, Ce) analogues,[10] where x is on the order of 3. The latter are cases, where evidently, both the electronic and geometric requirements are satisfied.

Phase Transitions. Variable temperature single-crystal X-ray diffraction data were collected for crystals of $RE_{5-x}Mg_xGe_4$ (RE = Gd, Tb, Dy, Ho). This was done to test if spontaneous temperature-induced phase transitions from one structure type to another exist. The lack of such transformations *above* the spontaneous magnetic ordering temperatures is evident even from their cell parameters, which show a nearly isotropic increase with volume expansion coefficients $\beta \approx 4 \times 10^{-5}\,K^{-1}$, and constant c/a ratios (Supporting Information, Tables S28−S39). Such thermal behavior is typical of the normal metals and intermetallic compounds and is different than those of some $RE_5(Si_xGe_{1-x})_4$ systems,[1−7] where heating and/or cooling in the paramagnetic regime can result in first-order phase transitions (concomitant to forming Si- or Ge-dimers, which is not the case here). For $Gd_{5-x}Mg_xGe_4$ (x = 1.45(1)), magnetic order occurs at around 110 K (vide infra), which allows for probing with a relative ease the single-crystal structure in the magnetically ordered state, *below* the spontaneous magnetic ordering temperature. Comparing the metrics of the structure at 90 K and at 120 K (Supporting Information, Table S31) suggests that no first-order phase transition takes place upon crossing the ordering temperature ; the c/a ratio remains constant, 1.087 in both cases, and the changes in the unit cell parameters corroborate the above-discussed thermal expansion behavior. Structure refinements at 90, 120, and 293 K confirm these conclusions (Supporting Information, Tables S31−S33).

Magnetic Properties. Field cooled (FC) and zero field cooled (ZFC) *dc* magnetization (M) measurements were completed for the whole series $Ho_{5-x}Mg_xGe_4$ ($1.23 \leq x \leq 2.08$), and the results are presented in Figure 3. As can be seen from the plots, there is a significant difference in the FC and ZFC curves, indicating a complex magnetic behavior. The $\chi(T)$ data in FC mode increase markedly below 30 K, reaching very high susceptibility values, about 5−16 emu/mol-Ho. The ZFC data, in turn, show sharp maxima around 17−24 K. Previous work has

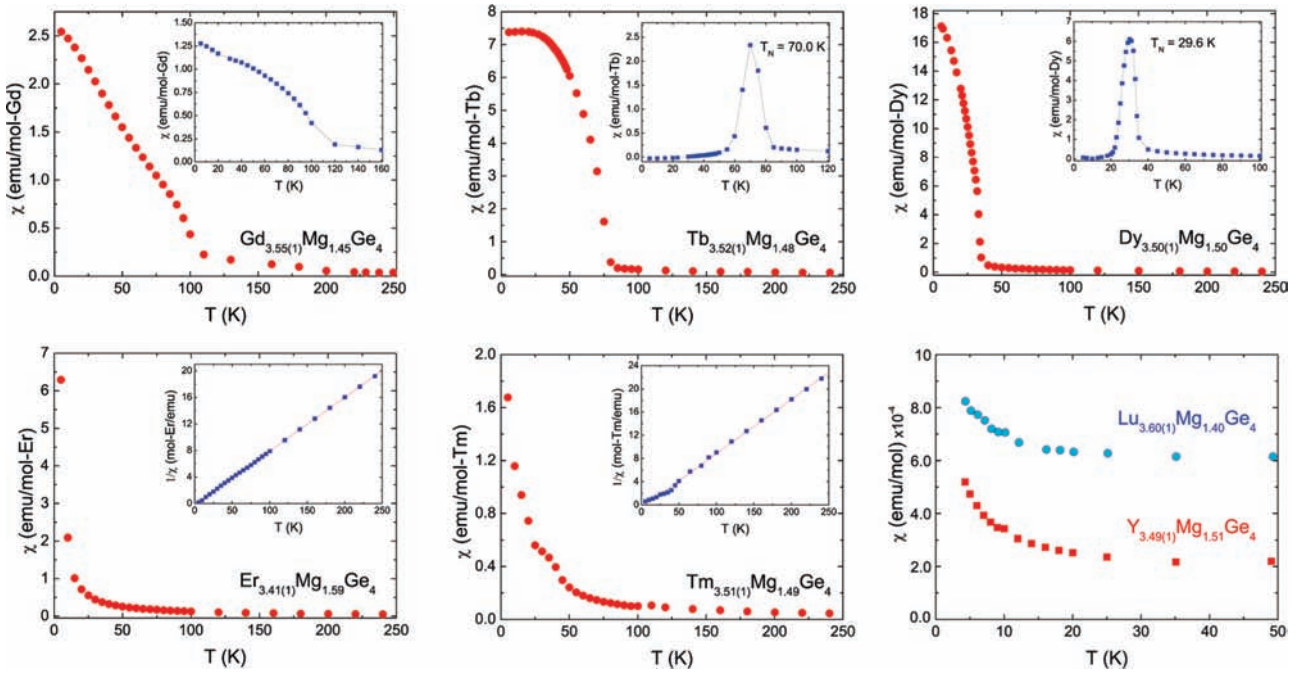

Figure 4. Magnetic susceptibility ($\chi = M/H$) vs temperature for the series $RE_{5-x}Mg_xGe_4$ (RE = Gd−Dy, Er, Tm, Lu, and Y). For the $RE_{5-x}Mg_xGe_4$ (RE = Gd−Dy) phases, which order magnetically, with (FC) measurements presented in the main panels and zero field cooled (ZFC) measurements presented in the insets. The corresponding Néel temperatures (T_N) from the ZFC plots are marked down. For the $RE_{5-x}Mg_xGe_4$ (RE = Er and Tm) phases, the main panels show the field cooled (FC) measurements, and the insets show the linear fits of the inverse susceptibility vs temperature. For the non-magnetic $RE_{5-x}Mg_xGe_4$ (RE = Lu and Y) phases, only the field cooled measurements are shown. All data are gathered in applied field of 100 Oe.

indicated that the bulk magnetization behavior of pure Ho_5Ge_4 shows similar characteristics with one study reporting an ordering temperature at 25 K and an anomaly at 18 K,[7] while a much earlier report gives an ordering temperature of 21 K.[33] These differences are likely due to the way the values have been determined (the applied magnetic fields are very different in both cases), or perhaps unrecognized impurities (which is not without a precedent, as discussed elsewhere [6]).

The large increase of the magnetic susceptibility in FC mode and the cusp-like features in all of the $\chi(T)$ data from the corresponding ZFC curves, support the coexistence of an antiferromagnetic and ferromagnetic component to the magnetic structure. This difficulty in clearly describing the magnetic ground state of the compounds crystallizing with this type is well documented. Of particular relevance to this work are the neutron diffraction experiments on Ho_5Ge_4,[29] which suggest that the magnetic structure is best described as two competing magnetic sublattices: (i) one, where the localized moments of the rare-earth metals are ferromagnetically coupled in layers that are parallel to the *ac*-plane, and (ii) another one, where the former layers are coupled to each other via strong antiferromagnetic interactions along the crystallographic *b*-axis. The presented data for $Ho_{5-x}Mg_xGe_4$ ($1.23 \leq x \leq 2.08$) and the fact the ZFC and FC curves are markedly different is consistent with this model; however, the availability of only polycrystalline samples did not allow for measurements in different directions to fully confirm the proposed magnetic structure. The corresponding ordering temperatures were thereby assigned as Curie temperature (T_C) in FC mode (determined from the midpoint in the jump in $d\chi/dT$), and Néel temperature (T_N) in ZFC mode (determined from the maximum of $\chi(T)$), and show that the transition temperatures in both instances decrease with increased Mg content. This can be related to parallel studies on La- and Y-doped Gd_5Ge_4 alloys,[12,17] where the dilution of the magnetic Gd^{3+} in the crystal structure with a non-magnetic La^{3+} or Y^{3+} also leads to lower ordering temperatures. The same is also true for samples of $Tb_{5-x}Mg_xGe_4$ and $Dy_{5-x}Mg_xGe_4$ with a different Mg content, the results for which are provided as Supporting Information.

For all six $Ho_{5-x}Mg_xGe_4$ specimens, both FC and ZFC curves show no difference at temperatures above 30 K, where the materials are paramagnetic and $\chi(T)$ obey the Curie−Weiss law $\chi(T) = C/(T - \theta_p)$ ($C = N_A\mu_{eff}^2/3k_B$ is the Curie constant and θ_p is the paramagnetic Weiss temperature).[34] Linear fits of the inverse susceptibility as a function of temperature yield effective magnetic moments on the order of 10.7−10.8 μ_B, in fairly good agreement with the value for a free-ion Ho^{3+} (10.60 μ_B), calculated from the Hund's rules.[34] Weiss temperatures are comparable to the apparent ordering temperatures and positive, which signals weak, ferromagnetic interactions between the Ho moments. Similarly complex low temperature magnetism is evidenced for the $RE_{5-x}Mg_xGe_4$ (RE = Gd, Tb, and Dy) phases, while $RE_{5-x}Mg_xGe_4$ (RE = Er and Tm) do not order magnetically down to 5 K (Figure 4). This is understandable since the ordering temperatures appear to follow the de Gennes factor $J(J + 1)(g - 1)^2$ of the specific lanthanide ion;[34] therefore, if the Er- and Tm-analogues undergo magnetic transitions, they should be at temperatures

(33) Holtzberg, F.; Gambino, R. J.; McGuire, T. R. *J. Phys. Chem. Solids* **1967**, *28*, 2283.

(34) Smart, J. S. *Effective Field Theories of Magnetism*; Saunders: Philadelphia, PA, 1966.

Table 5. Selected Magnetic Data for $RE_{5-x}Mg_xGe_4$ (RE = Gd−Tm, Lu and Y)

compound [a]	T_N (K)	θ_p (K)	μ_{calcd} (μ_B)	μ_{eff} (μ_B)
$Y_{3.49(1)}Mg_{1.51}Ge_4$	Pauli paramagnetism			
$Gd_{3.55(1)}Mg_{1.45}Ge_4$	110	42	7.94	8.30
$Tb_{3.52(1)}Mg_{1.48}Ge_4$	70	19	9.72	9.97
$Dy_{3.50(1)}Mg_{1.50}Ge_4$	31	8	10.65	10.85
$Ho_{3.62(1)}Mg_{1.38}Ge_4$	23	6	10.61	10.75
$Er_{3.41(1)}Mg_{1.59}Ge_4$		3	9.58	9.92
$Tm_{3.51(1)}Mg_{1.49}Ge_4$		1	7.56	8.15
$Lu_{3.60(1)}Mg_{1.40}Ge_4$	Pauli paramagnetism			

[a] Although attempts were made to synthesize samples with the same composition, there are small differences in the refined formulas, which make difficult the direct comparison of the trends across the family.

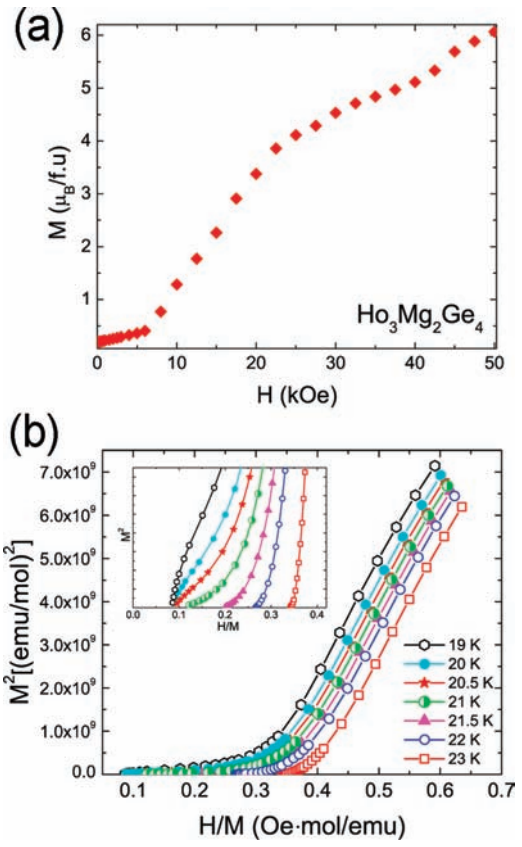

Figure 5. (a) Magnetization (M) vs applied field (H) for $Ho_{3.05(1)}Mg_{1.95}Ge_4$, measured at 2 K. (b) Arrot plots (M^2 vs H/M) for $Ho_{3.05(1)}Mg_{1.95}Ge_4$. The magnetization isotherms were collected in the temperature interval 19 to 23 K, with 0.5 K increments.

below 5 K. $Lu_{5-x}Mg_xGe_4$ and $Y_{5-x}Mg_xGe_4$ are Pauli-like paramagnetic, as expected for compounds with no localized f-electrons. Plots of the FC and the ZFC magnetic susceptibility versus temperature for the compounds that undergo magnetic order, as well as the FC magnetic susceptibility for the remaining ones, are presented in Figure 4; important magnetic parameters for selected samples of $RE_{5-x}Mg_xGe_4$ with close compositions are given in Table 5.[35]

To further study the competing long-range ferromagnetic and antiferromagnetic order, thorough magnetic isotherm measurements were undertaken for $Ho_3Mg_2Ge_4$. Attempts to saturate the magnetic moments were undertaken (Figure 5a), but as seen from the plot, the magnetization as a function of an applied field up to 50 kOe shows no saturation. The maximum saturation moment is 6 μ_B per formula unit, much lower than that expected gJ value of 10 μ_B for free-ion Ho^{3+}. Similar findings are reported for Ho_5Ge_4 and are attributed to the slow alignment of Ho moments in the non-collinear magnetic structure.[36] The three steps in the isotherm, at about 7, 22, and 42 kOe are suggestive of field-induced magnetic phase transitions.[36] Analogous field-dependence and very low saturation moment were obtained for $Gd_{5-x}Mg_xGe_4$, $Tb_{5-x}Mg_xGe_4$, and $Dy_{5-x}Mg_xGe_4$ as well, and the corresponding plots are presented in the Supporting Information section. On the basis of the previously discussed low temperature structures, we argue that crystallographic phase transitions are unlikely explanation for such behavior, although they cannot be completely ruled out in the absence of structural data at low temperature in applied magnetic fields.

Additional field-dependent magnetization measurements in the range of temperatures from 19 to 23 K, chosen in close proximity to the transition temperature of $Ho_3Mg_2Ge_4$, were also completed. From the gathered M vs H data, the H/M isotherms were plotted as a function of M^2, commonly referred to as an Arrott plot (Figure 5b).[37] Representation of the data in this way provides additional information concerning the observed magnetic behavior. For instance, the shape of the presented plots is characteristic of systems that exhibit ferromagnetic interactions but do not have a clearly defined ferromagnetic ground state.[38] This corroborates the previously discussed complex magnetic structure, brought about via strong RKKY coupling of the f-electrons of the lanthanide atoms occupying crystallographically inequivalent positions. Another possible way of explaining this, as seen in the case of Gd_5Ge_4, is the Landau theory, which can account for the existence of ferromagnetic $RE-RE$ interactions alongside antiferromagnetism.[39] Indeed, a number of studies demonstrate the formation of "ferromagnetic clustering" or Griffiths phases in compounds such as $Tb_5Si_2Ge_2$ and Dy_5Si_3Ge, among others.[40] Of interest to this discussion is also the fact that one of the rare-earth atoms is completely replaced by non-magnetic Mg does not change in a

(35) The effective magnetic moments are somewhat higher that the expected moments for a free ion, almost certainly because of small amounts of secondary phases present.

(36) Prokleska, J.; Vejpravová, J.; Sechovsky, V. *J. Magn. Magn. Mater.* **2007**, *316*, 313.
(37) Arrott, A. *Phys. Rev.* **1957**, *108*, 1394.
(38) (a) Brommer, P. E. Franse, J. J. M. In *Ferromagnetic Materials*; Buschow, K. H. J., Wohlfarth, E. P., Eds.; North Holland: Amsterdam, 1990; Vol. 5, p 323.(b) Jia, S.; Ni, N.; Samolyuk, G. D.; Safa-Sefat, A.; Dennis, K.; Ko, H.; Miller, G. J.; Bud'ko, S. L.; Canfield, P. C. *Phys. Rev. B* **2008**, *77*, 104408. (c) Yeung, I.; Roshko, R. M.; Williams, G. *Phys. Rev. B* **1986**, *34*, 3456. (d) Yuhasz, W. M.; Frederick, N. A.; Ho, P.-C.; Butch, N. P.; Taylor, B. J.; Sayles, T. A.; Maple, M. B.; Betts, J. B.; Lacerda, A. H.; Rogl, P.; Giester, G. *Phys. Rev. B* **2005**, *71*, 104402. (e) Padmanabhan, B.; Bhat, H. L.; Elizabeth, S.; Röβler, S.; Röβler, U. K.; Dörr, K.; Müller, K. H. *Phys. Rev. B* **2007**, *75*, 024419.
(39) Levin, E. M.; Gschneidner, K. A.Jr.; Lograsso, T. A.; Schlagel, D. L.; Pecharsky, V. K. *Phys. Rev. B* **2004**, *69*, 144428.
(40) (a) Magen, C.; Algarabel, P. A.; Morellon, L.; Araújo, J. P.; Ritter, C.; Ibarra, M. R.; Pereira, A. M.; Sousa, J. B. *Phys. Rev. Lett.* **2006**, *96*, 167201. (b) Nirmala, R.; Mudryk, Ya.; Pecharsky, V. K.; Gschneidner, K. A., Jr. *Phys. Rev. B* **2007**, *76*, 104417.

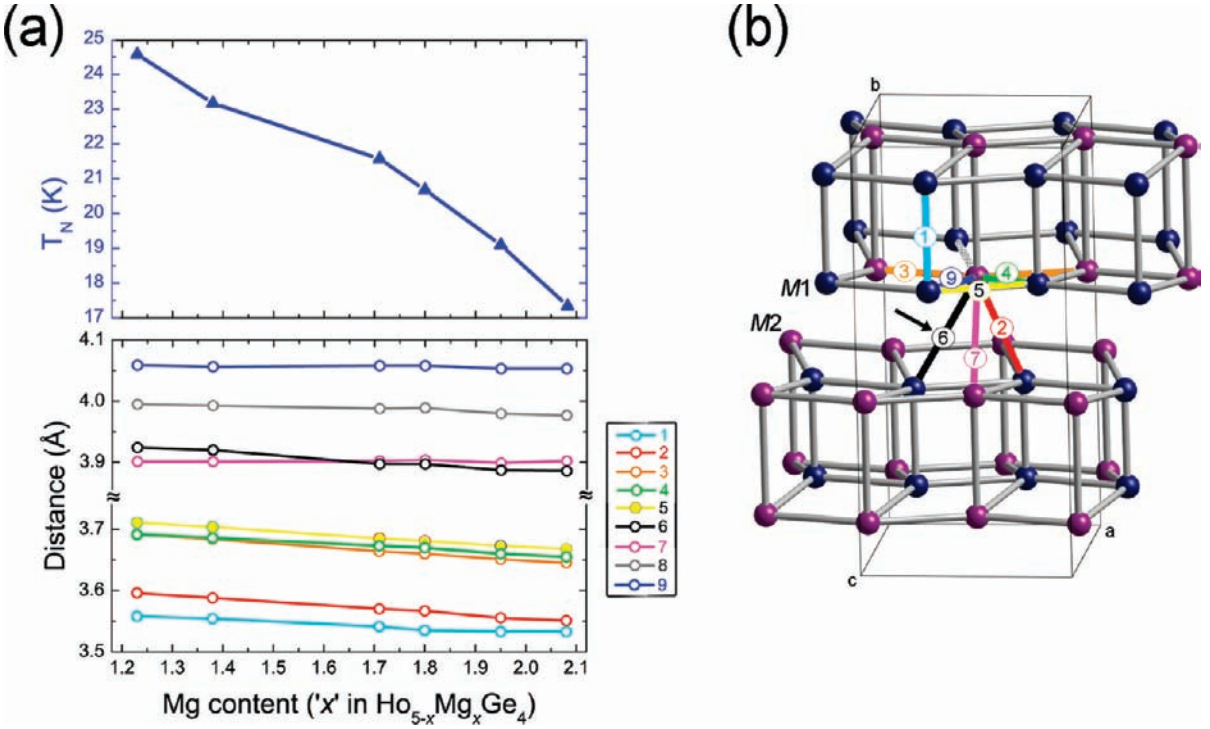

Figure 6. (a) Variations of Néel temperatures of the $Ho_{5-x}Mg_xGe_4$ ($1.23 \leq x \leq 2.08$) phases as a function of the Mg content alongside the variations of the Ho−Ho distances. (b) Schematic view of the Ho sub-structure, highlighting the different metal−metal distances. The $M1-M2$ which experiences about 12% change as the Mg content increases is marked down with an arrow. The considered Ho−Ho distances are color-coded.

significant way the magnetic interaction, which implies that the coupling between the rare-earth cations in the 4*c* sites is different than the coupling in the neighboring slabs.

Plotting the field-dependent data in such a way allows for the determination with greater certainty of the Curie temperature as well. For this purpose, the linear portion of the isotherm (H/M) which, when extrapolated to intersect the origin, corresponds to the Curie temperature. As seen from the inset provided in Figure 5b, the isotherms measured at temperature of 20.5 and 21 K can be crudely extrapolated via a linear fit to pass through the zero, while the isotherms representing the temperatures above and below, show much greater deviations from linearity near the origin of the plot. This confirms the Curie temperature extracted from the data shown in Figure 3.

An interesting correlation of the Néel temperatures for the series $Ho_{5-x}Mg_xGe_4$ ($1.23 \leq x \leq 2.08$) with the Mg content is depicted in Figure 6—higher Mg content and lower valence electron concentration result in a gradual decrease of the Néel temperature from the antiferromagnetic structure. The same trend is followed by the Curie temperatures from the corresponding FC curves as well. Apparently, increased Mg content not only strengthens the Ge3−Ge3 bonding but also leads to shortening of certain Ho−Ho distances, while others remain virtually unchanged. This point is demonstrated on the accompanying plot, showing the dependence of the metal−metal interactions with "*x*". Attention is drawn to two $M1-M2$ and $M1-M1$ contacts, both of which represent interactions between neighboring rare-earth metal slabs along the crystallographic *b*-direction (Figure 6b). Such counteracting behavior could have a strong effect on the two co-existing magnetic lattices and could be the most likely factor for the observed variations in the magnetic ordering temperatures of the members of the $Ho_{5-x}Mg_xGe_4$ series. Comparing the Ho−Ho contacts in pure Ho_5Ge_4 and in its Mg-substituted derivatives emboldens these speculations—the typical contraction of the metal−metal distances is on the order of 3 to 8%, while the above-mentioned $M1-M2$ contacts are shortened by nearly twice as much (Figure 6).

Conclusions

A series of ternary rare-earth metal magnesium germanides, $RE_{5-x}Mg_xGe_4$ ($x \approx 1.0-2.3$; RE = Gd−Tm, Lu, Y), have been synthesized and structurally characterized. They further demonstrate the ability of the Gd_5Si_4 structure to adapt to varied electron count through the substitution of a trivalent rare-earth metal with the divalent Mg. The site preference observed in the structure shows that the smaller Mg atoms preferentially occupy the 4*c* sites at the center of a distorted octahedron of Ge atoms, inscribed within a cube of rare-earth metal atoms. One of the latter sites also shows a small admixture of Mg, allowing for a sizable homogeneity range. The Mg-content influences the structural characteristics and the observed physical properties. Most notably, specific Ge−Ge interactions are strengthened as more Mg substitutes the rare-earth metal. The Gd, Tb, Dy, and Ho compounds order magnetically at low temperatures, and their magnetic structure likely boast two co-existing magnetic states—ferromagnetic and antiferromagnetic. In addition, the Mg-content has been shown to have an effect on the magnetic properties of the compounds where a decrease in the corresponding Néel or Curie temperatures occurs for Mg-richer samples because of the dilution of the magnetic lanthanide atoms.

These studies also emphasize the ability for the Gd_5Si_4 type structure to accommodate a variety of non-magnetic atoms in wide ranges, thereby allowing for systematic investigations of structural trends and properties of interest. Currently, ongoing efforts include extending this chemistry to other alkali/alkaline-earth elements.

Acknowledgment. Svilen Bobev acknowledges financial support from the National Science Foundation through Grant DMR-0743916 (CAREER). P.H.T. thanks the University of Delaware for the University Graduate Fellowship and the International Centre for Diffraction Data (ICDD) for the Ludo Frevel Crystallography Scholarship. Work at LANL was done under the auspices of the U.S. DOE.

Supporting Information Available: A combined X-ray crystallographic file in CIF format, along with details of the synthesis, comprehensive tables with crystallographic information, a representation of the crystal structure with anisotropic displacement parameters, powder pattern with calculated and observed intensities, additional magnetization data. This material is available free of charge via the Internet at http://pubs.acs.org.